Int J Adv Manuf Technol (2008) 35:1124–1135
DOI 10.1007/s00170-006-0794-x

ORIGINAL ARTICLE

Manufacturing models for design and NC grinding of truncated-cone ball-end cutters

Jone-Ming Hsieh

Received: 9 December 2005 / Accepted: 4 September 2006 / Published online: 12 December 2006

Abstract This paper presents a set of mathematical models for the design and manufacture of the helical flute and cutting-edge curve of a pair of truncated-cone ball-end cutters. The section profile and relative feeding velocities of the grinding wheel in NC machining of the cutter are deduced. In addition, the deviation of the cutting-edge curve, residual material and the land lack caused by the modified radial feeding velocity are taken into consideration. In order to finish the residual material and rebuild the land of the cutter, the technique for compensation has been developed in this research. The accuracy of the theoretical models is verified by means of an experimental machining test using a WALTER CNC grinding machine. The experimental results are in good agreement with those predicted theoretically, thereby confirming the accuracy and reliability of the proposed models. This study serves as a valuable reference for researchers investigating the NC machining of cutters with special forms.

Keywords Helical flute · NC grinding · Cutting-edge · Inverse problem

1 Introduction

With the increase of tasks for machining complex surfaces and the rapid development of NC machining technology, revolving tools have been widely used in NC machining of complex surfaces. There are different kinds of revolving tools with different applications. The applications and NC machining properties of ball-end cutters, flat-end cutters and toroidal cutters have been introduced in many references [2, 3, 5]. Nowadays, revolving tools are essential for NC machining. Since helical cutting-edges help improve machining properties, increasing a tool's life and enhancing a tool's properties, design and NC grinding of helical flute and cutting-edge curve have become important research subjects.

Helical flute NC machining is a widely used process in order to generate a helical swept flute on cylindrical workpieces using grinding wheel. Agullo-Battle et al. [1] worked on the design of milling cutters or grinding wheels for twist drill flute machining. Splines were defined and used to link the neighboring span smoothly. Sheth and Malkin [9] investigated the direct and inverse problems and also analyzed the dynamic properties related to machining parameters including the depth of cut, feed rate, contact arc-length, and tool point velocity. For the analytical resolution of this problem through a CAD approach, a generalized helical flute machining model, utilizing the principles of differential geometry and kinematics, has been developed by Ehmann (1996) [4, 6].

According to engineering demands, some of the research focused on at the design concepts and mathematical models without investigating the NC grinding process. Though NC grinding has been investigated [6], the approach focused on NC grinding of cutting-edge curves or rake faces individually without simultaneously investigating the NC grinding process for machining the whole helical flute surface. Liu [7] discussed the cutting edge on the special revolving cutter. Zhang and Yao [11] presented the algorithm of cutting edge of cutter with a constant helical angle. Tang and Chen [10] have investigated the models for 2-axis NC machining of cutter. Liu and Liu [8] have presented the mathematical model of the helical flute of cone-type ball-

J.-M. Hsieh (✉)
Department of Mechanical Engineering, Cheng Shiu University,
83342 Kaohsiung, Taiwan, Republic of China
e-mail: jone.ming@gmail.com

end cutter. Tsai and Hsieh [12] derived a design and NC manufacturing model of ball-end cutters. Chen et al. [13–16] presented a set of mathematical models for design and manufacture of the helical flute, cutting-edge curve, and grinding wheel for concave-arc ball-end milling cutters. Tsai and Hsieh [17] investigated the influences of a variety of cutting-edge curves upon the Inconel 718 machining process. Although the correlative research delves more and more deeply, problems still exist and the major shortcoming of the existing approaches is their lack of generality and systematization.

This paper discusses most of the questions of the cutter, such as design, manufacture, simulation and compensation. A series of general models of revolving cutters, including cutting edge, flute section and relative velocities of grinding wheel, are also presented. The manufacture of the basic flute is finished mainly in once by 2-axis NC machining. The correlative models and results will be introduced as follows.

2 Design of the cutting edge of revolving cutter

The axial cross-section profile and geometric parameters for a truncated-cone, ball-end cutter are shown in Fig. 1. Obviously, the tool is composed of a cylindrical shank, a truncated-cone and a spherical-head. In helical flute machining, the surfaces of revolution to be machined should be surfaces with a helical cutting-edge, i.e., the truncated-cone and spherical-head. In this paper, a revolving tool with four helical flutes is considered. The desired helical cutting-edge makes the constant helical angle ψ to a generatrix. The spherical surface can be expressed by:

$$\mathbf{r} = \left\{ \sqrt{R^2 - z^2}\cos\phi, \sqrt{R^2 - z^2}\sin\phi, z \right\} \tag{1}$$

where $z \in [-R, -R\sin\alpha]$.

In obtaining the mathematical model of desired helical cutting-edge, the first fundamental forms of surfaces should be calculated. To compute the first fundamental forms of surfaces, we notice that

$$\mathbf{r}_z = \left\{ \frac{-z}{\sqrt{R^2 - z^2}}\cos\phi, \frac{-z}{\sqrt{R^2 - z^2}}\sin\phi, 1 \right\}$$
$$\mathbf{r}_\phi = \left\{ -\sqrt{R^2 - z^2}\sin\phi, \sqrt{R^2 - z^2}\cos\phi, 0 \right\}.$$

The coefficients of the first fundamental form can be obtained as Eq. (2):

$$\begin{cases} E = \mathbf{r}_z^2 = \frac{R^2}{R^2 - z^2} \\ F = \mathbf{r}_z \cdot \mathbf{r}_\phi = 0 \\ G = \mathbf{r}_\phi^2 = R^2 - z^2. \end{cases} \tag{2}$$

Let the tangent vector of cutting edge be $d\mathbf{r}$ and the tangent vector of the generatrix be $\delta\mathbf{r}$ at the intersecting point. It is known that

$$\begin{cases} d\mathbf{r} = \mathbf{r}_z dz + \mathbf{r}_\phi d\phi \\ \delta\mathbf{r} = \mathbf{r}_z \delta z \end{cases} \tag{3}$$

Let the helical angle of the cutting edge be denoted as ψ. Base on the definition of the angle between two curves on the surface, we can obtain the following equations:

$$\frac{\cos^2\psi = \left(\frac{d\mathbf{r}\cdot\delta\mathbf{r}}{|d\mathbf{r}||\delta\mathbf{r}|}\right)^2 = \frac{Edz^2}{Edz^2 + Gd\phi^2}}{d\phi = \tan\psi\sqrt{\frac{E}{G}}dz = \frac{R}{R^2 - z^2}\tan\psi dz} \tag{4}$$

After integration

$$\phi = \frac{1}{2}\tan\psi \ln\frac{R+z}{R-z} + \phi_0 \tag{5}$$

where ϕ_0 is the initial value of parameter ϕ and equal to zero corresponding to z=0.

At the conjunction strip between the sphere part and the conic surface of the cutter, $z=-R\sin\alpha$, Eq. (5) becomes:

$$\phi_0 = \frac{1}{2}\tan\psi \ln\frac{1-\sin\alpha}{1+\sin\alpha} \tag{6}$$

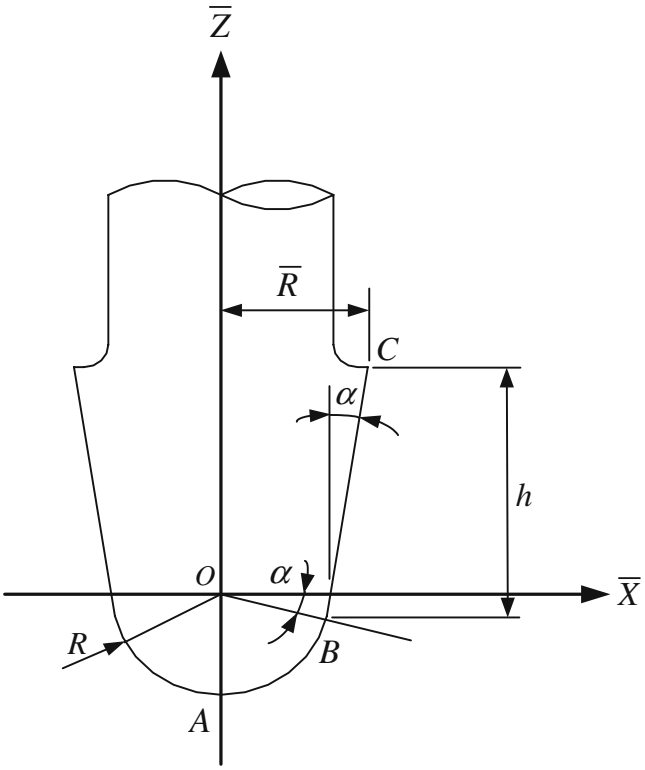

Fig. 1 Revolving surfaces, axial cross-section profile and geometric parameters for designed revolving tool

The conic surface can be expressed as following:

$$\mathbf{r}_1 = \{(R\cos\alpha + z_1\tan\alpha)\cos\phi_1, (R\cos\alpha + z_1\tan\alpha)\sin\phi_1, (z_1 - R\sin\alpha)\} \tag{7}$$

where $z_1 \in [0, h]$. Similarly, it is known that:

$$d\phi_1 = \frac{\tan\psi\sec\alpha}{R\cos\alpha + z_1\tan\alpha}dz_1 \tag{8}$$

After integration,

$$\phi_1 = \tan\psi\csc\alpha\ln(R\cos\alpha + z_1\tan\alpha) + C$$

According to the continuity of the cutting edge, $z=-R\sin\alpha$ when $z_1=0$, i.e.,

$$C = \phi_0 - \tan\psi\csc\alpha\ln(R\cos\alpha)$$

Therefore, the following equation can be obtained,

$$\phi_1 = \tan\psi\left(\csc\alpha\ln\frac{(R\cos\alpha + z_1\tan\alpha)}{R\cos\alpha} + \frac{1}{2}\ln\frac{1-\sin\alpha}{1+\sin\alpha}\right) \tag{9}$$

3 Preliminary design of feeding velocity in NC grinding

Since the influence of grinding radial depth and axial velocity on the helical flute surface should be taken into consideration, the radial feeding velocity should not be determined until the profile of grinding wheel has been made. The workpiece is assumed to rotate about the **Z** axis of the machine frame with an angular velocity ω

$$\frac{d\phi}{dt} = \omega = \text{constant} \tag{10}$$

and at the same time, the axial velocity with respect to spherical surface is

$$V_z = \frac{dz}{dt} = \frac{R^2 - z^2}{R\tan\psi}\frac{d\phi}{dt} = \omega\cot\psi\frac{R^2 - z^2}{R} \tag{11}$$

Simultaneously, the axial velocity with respect to conical surface should be

$$V_{z_1} = \frac{dz_1}{dt} = \omega(R\cos\alpha + z_1\tan\alpha)\cos\alpha\cot\psi \tag{12}$$

At the conjunction strip between the sphere part and the conic surface, it is obvious that $z=-R\sin\alpha$ and $z_1=0$. Substitute into Eq. (11) and Eq. (12) for continuity check. It follows

$$V_{z_1} = V_z = R\omega\cos^2\alpha\cot\psi \tag{13}$$

Therefore, the continuity of cutting-edge is proved.

4 Geometry model of flute section profile

As shown in Fig. 2, the proposed cross-section profile of helical flute is formed by five segments and described as following:

- segment A_1B_1 forms the rake face with radial rake angle γ;
- circular arc B_1C_1 with radius $\overline{r_1}$ is applied to circumflex chip;

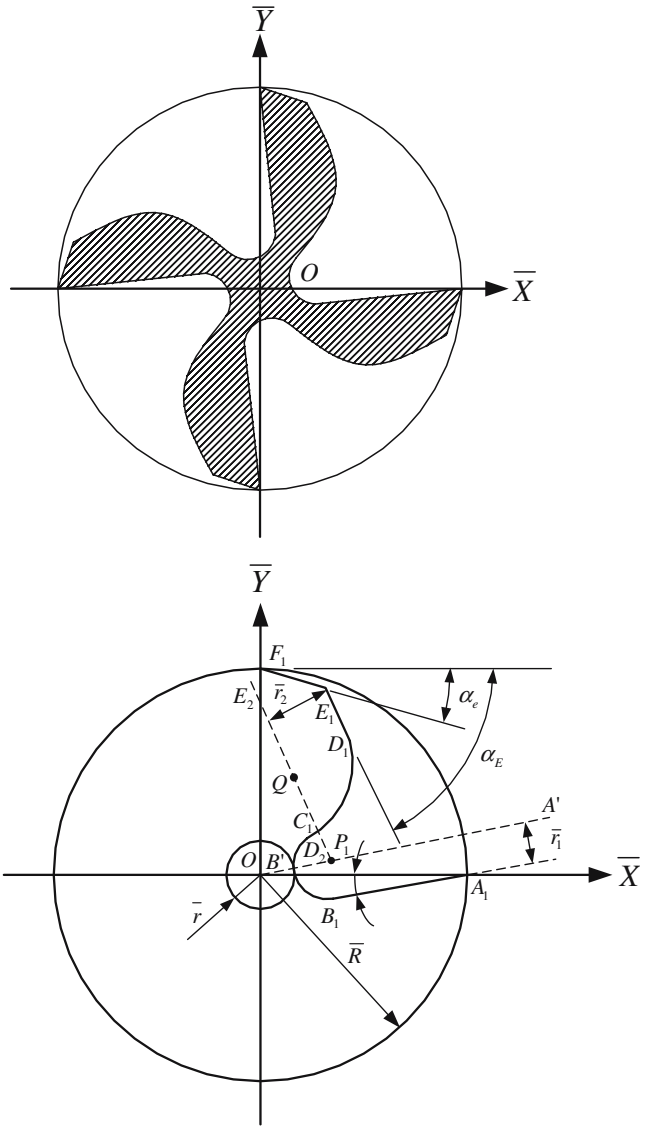

Fig. 2 Cross-section profile of groove

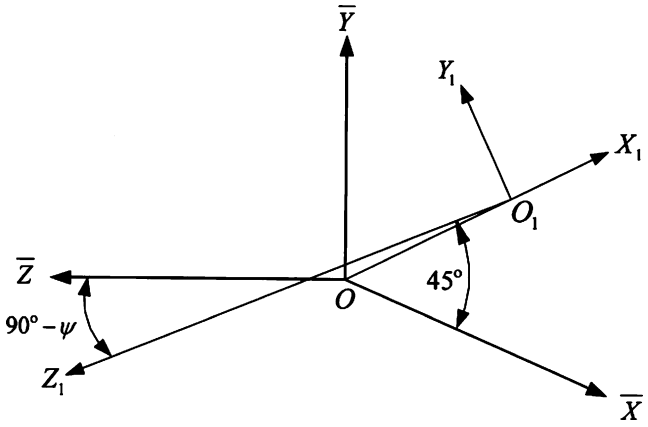

Fig. 3 Relationship between tool frame and grinding wheel coordinate systems

- circular arc C_1D_1 with radius $\overline{r_2}$ should be determined based on the smoothness for chip flow and required strength of tooth;
- segment D_1E_1 forms the secondary land, enhancing the strength of tooth with secondary relief angle α_E;
- segment E_1F_1 forms land with relief angle α_e;

In order to guarantee the strength of cutter, arbor should not be ground. Let the radius of arbor be $\overline{r}$. Besides, the consideration of the influence of variant flute profile on solving the geometry of grinding wheel, the cross-section of the designed flute profile corresponding to the conical part with a maximum radius has been chosen as the geometrical model for solving this inverse problem. We denote the radius of outer arbor to be $\overline{R}$. The geometry model of cross-section profile of helical flute is described as follows:

$$\overline{R} = R\cos\alpha + h\tan\alpha \tag{14}$$

Obviously, segment A_1B_1 can be described as

$$\mathbf{r}_{A_1B_1} = \{\overline{R}\ ,\ 0\} + \lambda_1\{-\cos\gamma\ ,\ -\sin\gamma\} \tag{15}$$

To obtain the equation of B_1C_1, the coordinate of center point P_1 should be determined first. Obviously, P_1 is an intersecting point between the line $A'B'$ parallel to segment A_1B_1 with a distance of $\overline{r_1}$ and the circle of radius $\overline{r} + \overline{r_1}$ centered at O. Therefore, from the simultaneous equations

$$\begin{cases} \mathbf{r}_{A'B'} = \{\overline{R} - \overline{r_1}\sin\gamma\ ,\ \overline{r_1}\cos\gamma\} + \lambda_1\{\cos\gamma\ ,\ \sin\gamma\} \\ \mathbf{r}_O = \{(\overline{r} + \overline{r_1})\cos\phi\ ,\ (\overline{r} + \overline{r_1})\sin\phi\}. \end{cases} \tag{16}$$

Fig. 4 Lack of flute in process of groove NC grinding without radial feeding

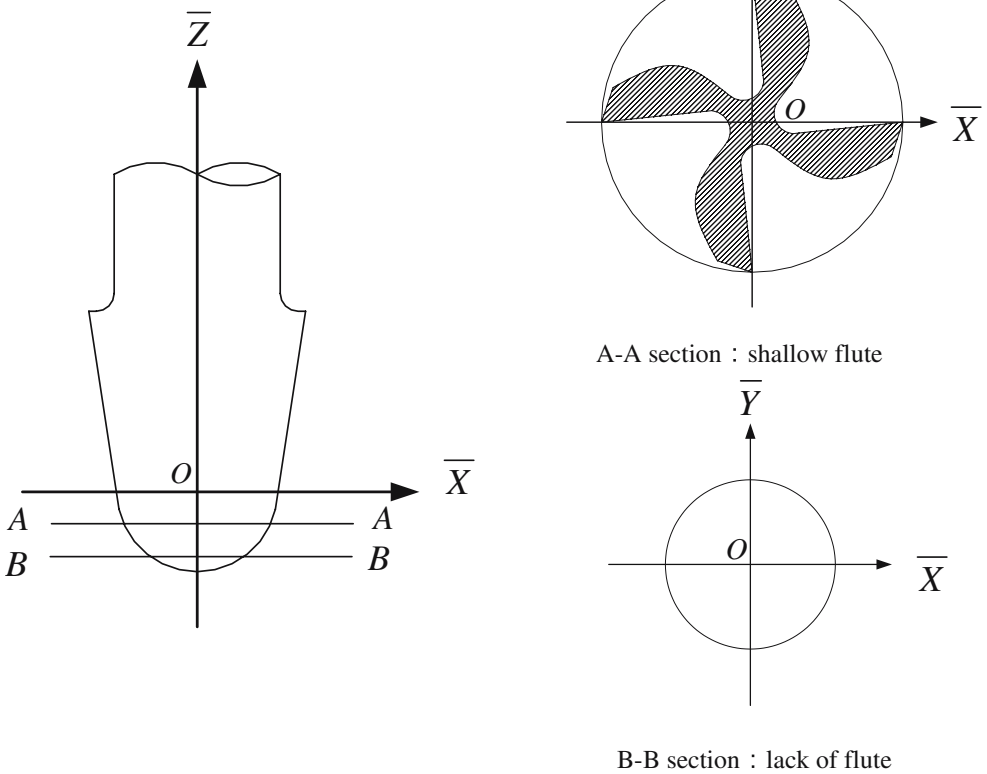

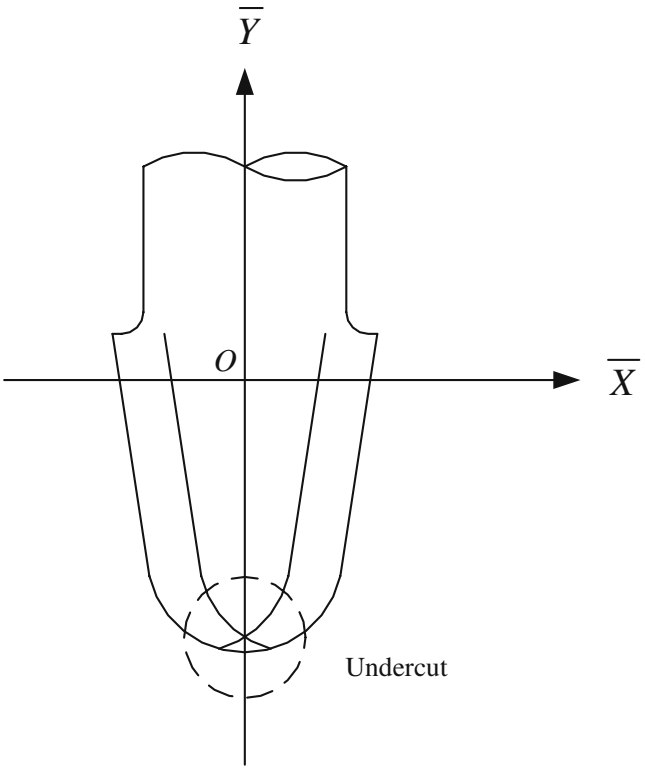

Fig. 5 Undercut in process of groove NC grinding while radial while feeding is equivalent to the decrement of sectional redius

λ_1 and ϕ can be obtained to determine $P_1(x_{P_1}, y_{P_1})$. Equation of $\overset{\frown}{B_1C_1}$ can be expressed to be:

$$\mathbf{r}_{\overset{\frown}{B_1C_1}} = \left\{x_{P_1} + \overline{r}_1 \cos\lambda_2 \ , \ y_{P_1} + \overline{r}_1 \sin\lambda_2\right\} \tag{17}$$

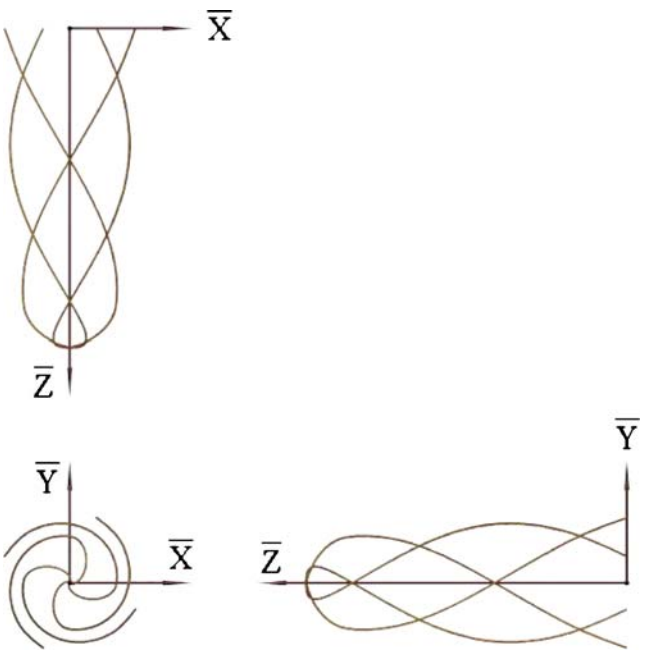

Fig. 6 The cutting-edge curve of the four-edge truncated-cone ball-end cutters

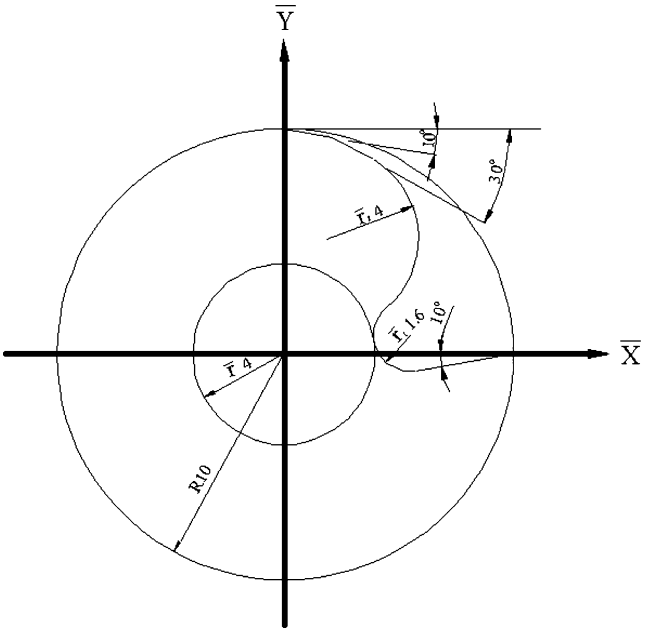

Fig. 7 The curve of groove shape cross-section for Table 2

and B_1 is the tangent point to circle B_1C_1 and segment A_1B_1. The coordinate of B_1 can be determined by solving the following equations:

$$\begin{cases} \mathbf{r}_{A_1B_1} = \left\{\overline{R} \ , \ 0\right\} - \lambda_1 \left\{\cos\gamma \ , \ \sin\gamma\right\} \\ \mathbf{r}_{\overset{\frown}{B_1C_1}} = \left\{x_{P_1} + \overline{r}_1 \cos\lambda_2 \ , \ y_{P_1} + \overline{r}_1 \sin\lambda_2\right\} \end{cases} \tag{18}$$

Let ℓ and α_e denote the length of land and the relief angle, respectively. Land E_1F_1 can be written in the form

$$\mathbf{r}_{E_1F_1} = \left\{0 \ , \ \overline{R}\right\} + \lambda_5 \left\{\cos\alpha_e \ , \ -\sin\alpha_e\right\} \tag{19}$$

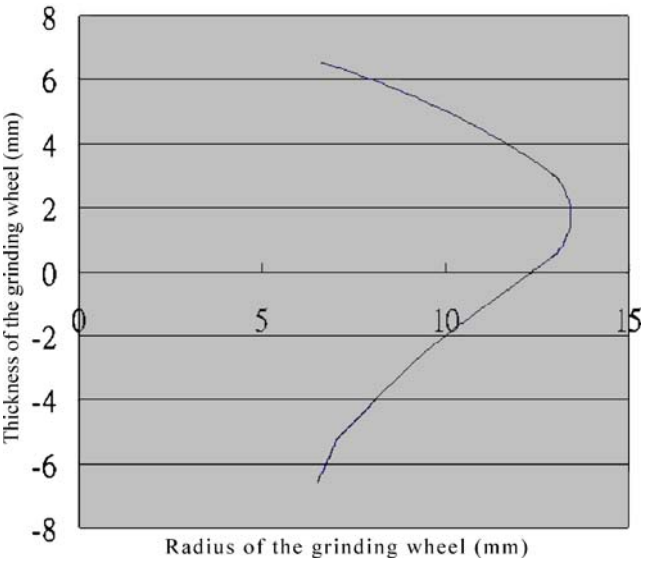

Fig. 8 The cross-section curve of the grinding wheel

Fig. 9 The computer simulation model of the grinding wheel

Hence, the coordinate of E_1 should be $(\ell\cos\alpha_e\ ,\ \overline{R}-\ell\sin\alpha_e)$, and so that D_1E_1 can be shown as

$$\mathbf{r}_{D_1E_1}=\left\{\ell\cos\alpha_e\ ,\ \overline{R}-\ell\sin\alpha_e\right\}+\lambda_4\{\cos\alpha_E\ ,\ -\sin\alpha_E\} \tag{20}$$

Circle C_1D_1 is tangent to segment D_1E_1 at point D_1 and is tangent to circle B_1C_1 at point C_1. Therefore, Q_1, center of the circle C_1D_1, is an intersecting point between the line D_2E_2 parallel to segment D_1E_1 with a distance of $\overline{r_2}$ and the circle CP_1 centered at P_1 with radius $\overline{r_2}+\overline{r_1}$. We obtain the equations

$$\begin{cases}\mathbf{r}_{D_2E_2}=\left\{\ell\cos\alpha_e-\overline{r_2}\sin\alpha_E\ ,\ \overline{R}-\ell\sin\alpha_e-\overline{r_2}\sin\alpha_E\right\}+\lambda_4\{\cos\alpha_E\ ,\ -\sin\alpha_E\}\\ \mathbf{r}_{CP_1}=\{x_{P_1}+(\overline{r_1}+\overline{r_2})\cos\phi_1\ ,\ y_{P_1}+(\overline{r_1}+\overline{r_2})\sin\phi_1\}.\end{cases} \tag{21}$$

By solving the solutions λ_4 and ϕ_1, the coordinate of $Q_1\left(x_{Q_1}\ ,\ y_{Q_1}\right)$ can be obtained and circle C_1D_1 is of the form

$$\mathbf{r}_{\overset{\frown}{C_1D_1}}=\left\{x_{Q_1}+\overline{r_2}\cos\lambda_3\ ,\ y_{Q_1}+\overline{r_2}\sin\lambda_3\right\} \tag{22}$$

Obviously, C_1 is the tangent point to circle B_1C_1 and circle C_1D_1. D_1 is the tangent point to circle C_1D_1 and segment D_1E_1. Thus, the coordinate of $C_1(x_{C_1}\ ,\ y_{C_1})$ can be obtained by solving the simultaneous Eq. (17) and (22). The coordinate of $D_1(x_{D_1}\ ,\ y_{D_1})$ can be found by solving the equation set of (20) and (22) simultaneously. The cross-section profile of designed flute in first quadrant can be formed by

$$\mathbf{r}_h=\{x(\lambda)\ ,\ y(\lambda)\}=\begin{cases}\left\{\overline{R}-\lambda_1\cos\gamma\ ,\ -\lambda_1\sin\gamma\right\}\ \lambda_1\in\left[\lambda_1^*\ ,\ \lambda_1^{**}\right]\\ \left\{x_{P_1}+\overline{r_1}\cos\lambda_2\ ,\ y_{P_1}+\overline{r_1}\sin\lambda_2\right\}\ \lambda_2\in\left[\lambda_2^*\ ,\ \lambda_2^{**}\right]\\ \left\{x_{Q_1}+\overline{r_2}\cos\lambda_3\ ,\ y_{Q_1}+\overline{r_2}\sin\lambda_3\right\}\ \lambda_3\in\left[\lambda_3^*\ ,\ \lambda_3^{**}\right]\\ \left\{\ell\cos\alpha_e+\lambda_4\cos\alpha_E\ ,\ \overline{R}-\ell\sin\alpha_e-\lambda_4\sin\alpha_E\right\}\ \lambda_5\in\left[\lambda_4^*\ ,\ \lambda_4^{**}\right]\\ \left\{\lambda_5\cos\alpha_e\ ,\ \overline{R}-\lambda_5\ \sin\alpha_e\right\}\ \lambda_5\in\left[\lambda_5^*\ ,\ \lambda_5^{**}\right].\end{cases} \tag{23}$$

Replacing λ_i by $\left[(\beta-i+1)\left(\lambda_i^{**}-\lambda_i^*\right)+\lambda_i^*\right]$ gives $r_i(\lambda_i)$ as $r_i(\beta)$. Hence, $\beta\in[i-1,i]$ for each part of $r_i(\beta)$, and consequently, Eq. (23) can be rewritten in the form given below by means of a unit step function, i.e.,

$$\begin{aligned}\mathbf{r}_h&=\{x(\beta),\ y(\beta)\}\\&=\sum_{i=1}^{5}r_i(\beta)[u(\beta-(i-1))-u(\beta-i)]\ ,\ \beta\in[0,5]\quad .\end{aligned} \tag{24}$$

Fig. 10 The original model of the grinding wheel

5 Design of the cross section of grinding wheel

The radial sectional radii of revolving surfaces are different for different coordinates z_i, and thus lead to different geometry of grinding wheel. However, it is impossible to use different grinding wheel for different sectional radius. In practice, flutes are sufficient with the effects such as chip circumflex, chip capacity, chip ejection, suitable rake angle for cutting and enough strength. Therefore, the methodology to determine the geometry of grinding wheel for a

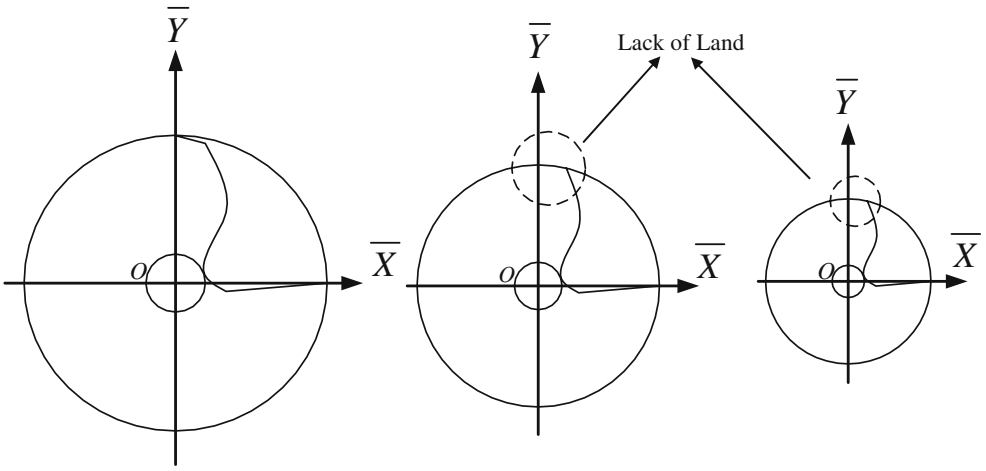

Fig. 11 Cross-section of groove that lack land

desired helical flute profile corresponding to section with radius $\overline{R}$ can meet the demand. Thus, the general equation of a helical surface, generated based on the given radial cross-section is obtained by rotating the cross-section around the **Z**-axis through an angle $\overline{\theta}$ as well as simultaneously translating it along the **Z**-axis through a distance $\left(\overline{R}\,\overline{\theta}\cot\psi\right)$. The helical flute surface equation for cylindrical cutter is obtained in the form:

$$\begin{aligned}\mathbf{r}^* &= \left\{x(t)\cos\overline{\theta} - y(t)\sin\overline{\theta}\ ,\ x(t)\sin\overline{\theta} - y(t)\cos\overline{\theta}\ ,\ \overline{R}\,\overline{\theta}\cot\psi\right\}\\ &= \left\{x^*\ ,\ y^*\ ,\ z^*\right\}\end{aligned} \tag{25}$$

where $\{x(t),\ y(t)\}$ is the cross-section profile defined in Eq. (23) and t, $\overline{\theta}$ represent the curvilinear coordinates of the surface.

To mathematically describe the relationship between the grinding wheel and the helical flute, two right-handed coordinate frames are introduced. As indicated in Fig. 3, coordinate system $\overline{\sigma} = \left[O\ ;\ \overline{\mathbf{X}}\ ,\ \overline{\mathbf{Y}}\ ,\ \overline{\mathbf{Z}}\right]$ represents the stationary machine frame. Coordinate system $\sigma_1 = [O_1\ ;\ \mathbf{x}_1\ ,\ \mathbf{y}_1\ ,\ \mathbf{z}_1]$ denotes the grinding wheel frame. Thus, z_1-axis in the stationary machine can be expressed by

$$\begin{aligned}\mathbf{r}_{Z_1} &= \left\{\frac{\sqrt{2}}{2}a\ ,\ \frac{\sqrt{2}}{2}a\ ,\ 0\right\}\\ &\quad+\overline{\lambda}\left\{\frac{\sqrt{2}}{2}\cos\psi\ ,\ -\frac{\sqrt{2}}{2}\cos\psi\ ,\ \sin\psi\right\}\end{aligned} \tag{26}$$

where a is the distance between the origins of frame $\overline{\sigma}$ and $\boldsymbol{\sigma}_1$, i.e., $OO_1 = a$ and should be larger than $\overline{R}$. $\overline{\lambda}$ is the length parameter of axis $O_1\mathbf{z}_1$.

According to the principle of inverse engineering of envelope, the common normal vector of any point on the

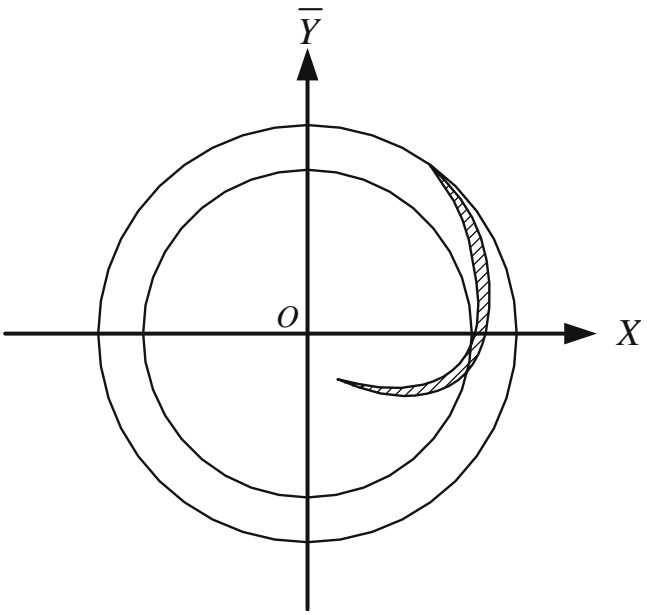

Fig. 12 Residual surface

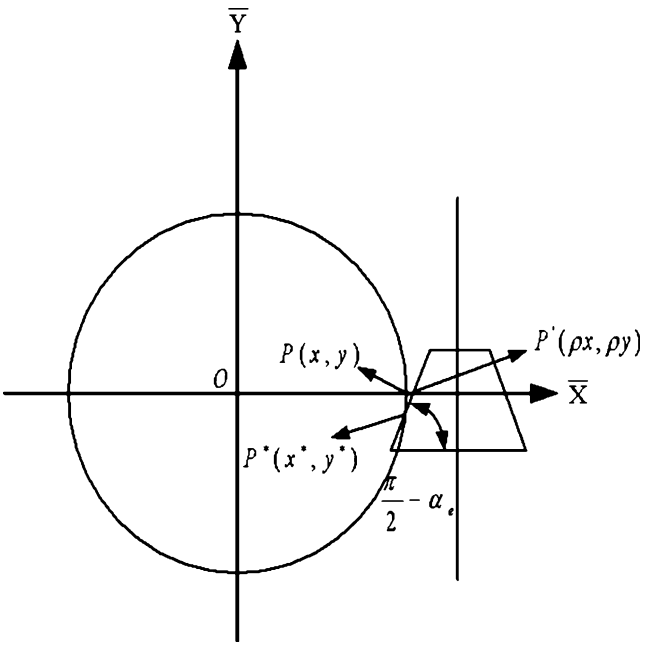

Fig. 13 The geometric parameters and coordinate system compensation of the grinding wheel

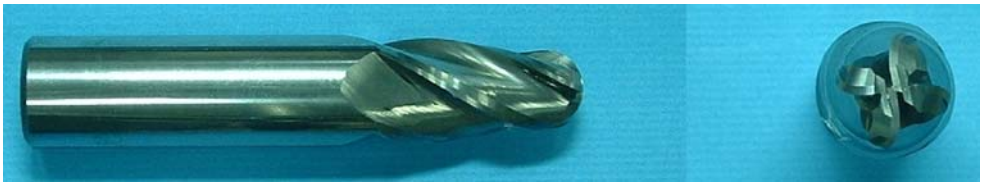

Fig. 14 The original model of the four-edge truncated-cone ball-end cutters (**a**) The cutting-edge curve of design (**b**) The cutting-edge curve of cutting (**c**) comparison

instant contact curve between the profile surface of grinding wheel and the spiral surface Eq. (25) must pass through the revolving axis O_1z_1 of the grinding wheel. The normal vector of an arbitrary point on the helical flute surface in the stationary machine frame is in the form

$$\widehat{\mathbf{r}} = \mathbf{r}^* + \overline{\mu}\mathbf{r}_t^* \times \mathbf{r}_{\overline{\theta}}^* = \left\{x^* + \overline{\mu}N_x \ , \ y^* + \overline{\mu}N_y \ , \ z^* + \overline{\mu}N_z\right\} \tag{27}$$

Where N_x, N_y, N_z are the fractions of the normal vector, and $\overline{\mu}$ is the length parameter of the normal vector.

Since the contact point between the grinding wheel and the helical flute surface must intersect the axis of the grinding wheel, the fractions of coordinates corresponding to Eq. (26) and Eq. (27) should be equal respectively at the intersecting points. In this way, the condition, which the points on the surface of Eq. (25) are also on the profile surface of the grinding wheel, can be defined. By utilizing the property of helical surface

$$y^*N_x - x^*N_y = bN_z \tag{28}$$

Where $b = \overline{R}\cot\psi$

Thus, the engagement relationship for grinding wheel and helical flute is formed as

$$a\left(\sqrt{2}N_z + N_y\tan\psi - N_x\tan\psi\right) + z^*\left(N_x + N_y\right) - N_z(x^* + y^*) + \sqrt{2}b\tan\psi N_z = 0 \tag{29}$$

By solving the engagement relationship Eq. (29), a nonlinear transcendental equation, in terms of $\overline{\theta}$ and substituting it into Eq. (21), the locus of the contact points is obtained and expressed as

$$\mathbf{r}^{**} = \left\{x(\overline{\theta}) \ , \ y(\overline{\theta}) \ , \ z(\overline{\theta})\right\} \tag{30}$$

The contact curve of Eq. (30) is on the profile surface of grinding wheel, transforming into coordinate system $\sigma_1 = \left[\overline{O_1} \ ; \ \mathbf{x}_1 \ , \ \mathbf{y}_1 \ , \ \mathbf{z}_1\right]$, by taking the following coordinate transformation

$$\begin{pmatrix} x_1 \\ y_1 \\ z_1 \\ t_1 \end{pmatrix} = \begin{pmatrix} 1 & 0 & 0 & -a \\ 0 & \sin\psi & \cos\psi & 0 \\ 0 & -\cos\psi & \sin\psi & 0 \\ 0 & 0 & 0 & 1 \end{pmatrix} \times \begin{pmatrix} \sqrt{2}/2 & \sqrt{2}/2 & 0 & 0 \\ -\sqrt{2}/2 & \sqrt{2}/2 & 0 & 0 \\ 0 & 0 & 1 & 0 \\ 0 & 0 & 0 & 1 \end{pmatrix} \begin{pmatrix} x(\overline{\theta}) \\ y(\overline{\theta}) \\ z(\overline{\theta}) \\ t \end{pmatrix} \tag{31}$$

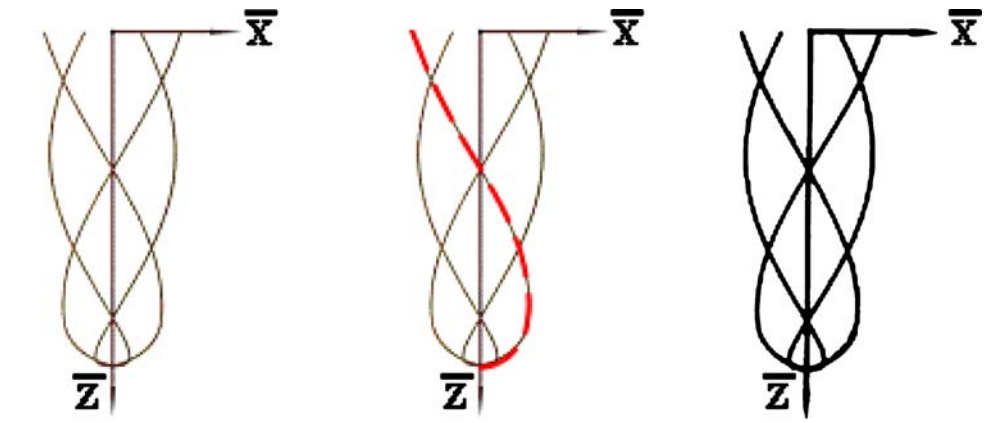

Fig. 15 The cutting-edge curve of cutting and those of design (**a**) The cross-section of the groove of the design (**b**) The cross-section of the groove of the cutting (**c**) comparison

(a) The cutting-edge curve of design (b) The cutting-edge curve of cutting (c) compare

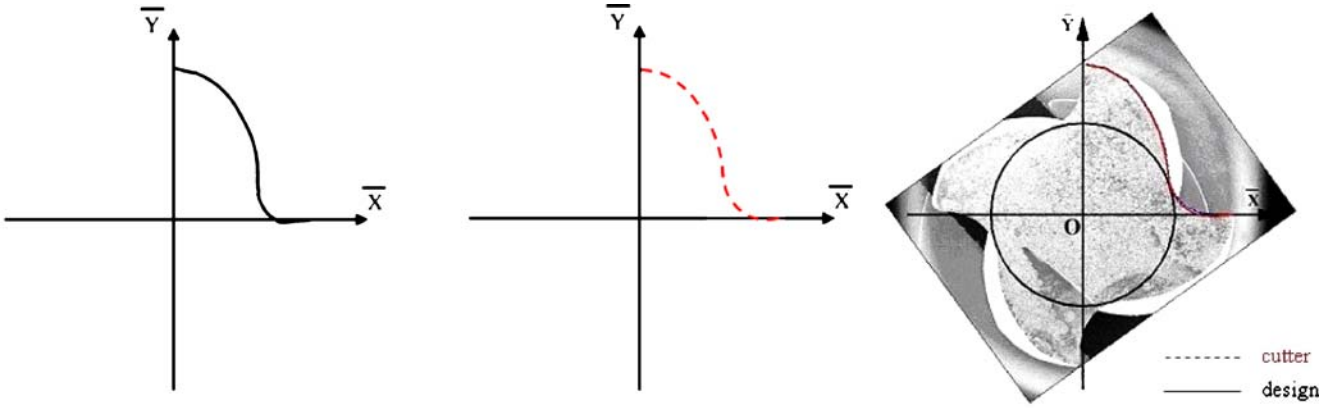

(a) The cross-section of groove of design (b) The cross-section of groove of cutting (c) compare

Fig. 16 The cross-section of the groove of the cutting and those of the design

By sweeping the contact curve around the $\mathbf{z}_1$-axis, the profile equation in the grinding wheel coordinate system can be expressed as

$$\begin{aligned}\mathbf{r}_{\overline{\varphi}} &= \left\{x_{\overline{\varphi}}, y_{\overline{\varphi}}, z_{\overline{\varphi}}\right\} \\ &= \{x_1 \cos\overline{\varphi} - y_1 \sin\overline{\varphi}, x_1 \sin\overline{\varphi} + y_1 \cos\overline{\varphi}, z_1\}\end{aligned} \tag{32}$$

then the intersecting curve between the profile surface Eq. (30) and the plane $y_1=0$ will be the profile curve of the grinding wheel, i.e.,

$$\begin{aligned}\mathbf{r}_c &= \{x_c\ ,\ 0\ ,\ z_c\} = \left\{\sqrt{x_{\overline{\varphi}}^2 + y_{\overline{\varphi}}^2}\ ,\ 0\ ,\ z_{\overline{\varphi}}\right\} \\ &= \left\{\sqrt{x_1^2 + y_1^2}\ ,\ 0\ ,\ z_1\right\}\end{aligned} \tag{33}$$

The motion of grinding wheel in the process of machining the flute must be designed with care. This is because that the profile of the grinding wheel is defined according to the spiral motion of flute on the cylinder surface, and the profile of designed cutter is not cylinder but a truncated-cone and spherical profile. With constant axial feeding, the helical flute of cylindrical cutter machined by the grinding wheel from Eq. (33) should be accurate under such relative frame. But for the designed cutter, the radial sectional radius is not constant so that the variance of radial feeding is inevitable and might cause undercut. In order to prevent such problems, the radial feeding velocity should be determined first, the machined helical flute should be verified, and the modification should be implemented.

6 Motion of the grinding wheel relative to workpiece

The radial feeding velocity of grinding wheel will affect the flute depth, the helical angle of the cutting edge and the happening of undercut. The following two cases must be treated carefully. One case is no radial feeding, as shown in Fig. 4. When the outer radius of the cutter section is less than $\overline{r}$, the flute is no longer existed. When the radius is greater but near $\overline{r}$, the flute depth is shallower. The second case, as shown in Fig. 5, is that undercut will happen while the radial feeding is equivalent to the decrement of sectional radius. When the radius of the cutter section is less than $\overline{R}-\overline{r}$, the maximal profile of the grinding wheel will grind through the axis of the cutter. Notice these two limit cases, the proper feeding amount of the grinding wheel should be determined according to the total variation of radius and the total variation of feeding amount. Let the radial displacement S_g vary proportionally to the variation $\overline{R}-\sqrt{x^2+y^2}$ of radius: Figs. 6, 7, 8, 9, 10, 11, 12, 13, 14, 15, 16

$$S_g = \overline{r} - \frac{\overline{r}}{\overline{R}}\sqrt{x^2+y^2} \tag{34}$$

If the radial feeding displacement is defined by Eq. (34), for spherical part, the equation of radial feeding velocity should be illustrated as:

$$v_g = \frac{dS_g}{dt} = -\frac{\overline{r}}{\overline{R}}\frac{d\sqrt{R^2-z^2}}{dt} = \frac{\overline{r}z\omega\cot\psi\sqrt{R^2-z^2}}{\overline{R}R} \tag{35}$$

Table 1 The cutting-edge curve geometrical parameters of the four-edge truncated-cone ball-end cutters

Parameters of the four-edge truncated-cone ball-end cutters	
Length of the truncated-cone ball-end cutters d	46.846 mm
Radius of the ball-end r	7.5 mm
Helical angle φ	30°
The diameter of the arbor be $2\overline{r}$	1.75 mm
Half conical angle α	5°
Modification parameter e	0.8
Length of the land b	2 mm
The maximal radius of cutter arbor to be $\overline{R}$	10 mm

Table 2 The geometry parameter of groove shape cross-section

Parameters of the groove shape cross-section			
The maximum radius of cuter arbor to be R	10 mm	The length land b	2 mm
The diameter of the arbor be $2\overline{r}$	8 mm	Relief angle α_e	$\pi/18$
The radius of the circumflex chip $\overline{r_1}$	1.6 mm	Secondary relief angle α_E	$\pi/6$
The radius based on the smoothness of chip flow $\overline{r_2}$	4 mm	Rake angle γ	$\pi/18$

For the conic surface,

$$v_{g_1} = -\frac{\omega\overline{r}}{\overline{R}}\tan\alpha\frac{\cot\psi(R\cos\alpha + z_1\tan\alpha)}{\sec\alpha} = -\frac{\omega\overline{r}}{\overline{R}}\sin\alpha\cot\psi(R\cos\alpha + z_1\tan\alpha) \tag{36}$$

At the conjunction boundary, $z=-R\sin\alpha$ and $z_1=0$, it is obvious that

$$v_g = -\frac{\omega\overline{r}}{\overline{R}}R\sin\alpha\cos\alpha\cos\psi = v_{g_1} \tag{37}$$

Equation (37) means that the radial feeding velocities are also continuous.

7 Manufacturing models for helical flute

By sweeping the axial cross-section of the required grinding wheel profile $\mathbf{r}_c$ around the $\mathbf{z}_1$-axis, the profile equation can be expressed in the coordinate system $\sigma_1 = \left[\overline{O_1}\,;\,\mathbf{x}_1\,,\,\mathbf{y}_1\,,\,\mathbf{z}_1\right]$ as following:

$$\widehat{\mathbf{r}} = \{\widehat{x}\,,\,\widehat{y}\,,\,\widehat{z}\} = \{x_c\cos\upsilon\,,\,x_c\sin\upsilon\,,\,z_c\} \tag{38}$$

We may now express the profile equation in terms of the machine coordinate system, $\overline{\sigma} = \left[\overline{O}\,;\,\overline{\mathbf{X}}\,,\,\overline{\mathbf{Y}}\,,\,\mathbf{Z}\right]$, by utilizing the relative coordinate transformation

$$\begin{cases} \widehat{x}^* = \frac{\sqrt{2}}{2}(\widehat{x}+a) - \frac{\sqrt{2}}{2}(\widehat{y}\sin\psi - \widehat{z}\cos\psi) \\ \widehat{y}^* = \frac{\sqrt{2}}{2}(\widehat{x}+a) + \frac{\sqrt{2}}{2}(\widehat{y}\sin\psi - \widehat{z}\cos\psi) \\ \widehat{z}^* = (\widehat{y}\cos\psi + \widehat{z}\,sin\,\psi) \end{cases} \tag{39}$$

Considering the effects of radial feeding S_g to $\widehat{x}^*$ and $\widehat{y}^*$, the equation of the grinding wheel profile is as following:

$$\begin{cases} \overline{x} = \widehat{x}^* + \frac{\sqrt{2}}{2}\left(\int v_g dt + C\right) = \widehat{x}^* + \frac{\sqrt{2}}{2}S_g \\ \overline{y} = \widehat{y}^* + \frac{\sqrt{2}}{2}\left(\int v_g dt + C\right) = \widehat{y}^* + \frac{\sqrt{2}}{2}S_g \end{cases} \tag{40}$$

Considering the effects of ω and v_z, the equation of group of the grinding wheel profile becomes

$$\begin{cases} x^* = \overline{x}\cos(\omega t) - \overline{y}\sin(\omega t) = \overline{x}\cos\phi - \overline{y}\sin\phi \\ y^* = \overline{x}\sin(\omega t) + \overline{y}\cos(\omega t) = \overline{x}\sin\phi + \overline{y}\cos\phi \\ z^* =^* + \int v_z dt + C =^* + z \end{cases} . \tag{41}$$

Thus, the condition for the intersecting surface envelope to exist is given by

$$\left(\mathbf{r}^*_{x_c}\,,\,\mathbf{r}^*_{\upsilon}\,,\,\mathbf{r}^*_z\right) = \begin{vmatrix} x^*_{x_c} & y^*_{x_c} & z^*_{x_c} \\ x^*_{\upsilon} & y^*_{\upsilon} & z^*_{\upsilon} \\ x^*_z & y^*_z & z^*_z \end{vmatrix} = 0 \tag{42}$$

Therefore, the practical flute surface can be expressed by follows:

Tables 1 and 2.

Therefore, the practical flute surface can be expressed by the following:

$$\begin{cases} \mathbf{r}^* = \{x^*, y^*, z^*\} \\ \left(\mathbf{r}^*_{x_c}, \mathbf{r}^*_{\upsilon}, \mathbf{r}^*_z\right) = 0 \end{cases} \tag{43}$$

Disregarding the deduction process, one can derive the practical obtained surface of the flute:

$$\begin{cases} \mathbf{r}^* = \{x^*, y^*, z^*\} \\ = \begin{cases} x^* = x_c\cos\upsilon\cos\left(\frac{\pi}{4}+\phi\right) - x_c\sin\upsilon\sin\psi\sin\left(\frac{\pi}{4}+\phi\right) \\ \quad +a\cos\left(\frac{\pi}{4}+\phi\right) + z_c\cos\psi\sin\left(\frac{\pi}{4}+\phi\right) + S_g\cos\left(\frac{\pi}{4}+\phi\right) \\ y^* = x_c\cos\upsilon\sin\left(\frac{\pi}{4}+\phi\right) + x_c\sin\upsilon\sin\psi\cos\left(\frac{\pi}{4}+\phi\right) \\ \quad +a\sin\left(\frac{\pi}{4}+\phi\right) - z_c\cos\psi\cos\left(\frac{\pi}{4}+\phi\right) + S_g\sin\left(\frac{\pi}{4}+\phi\right) \\ z^* = x_c\sin\upsilon\cos\psi + z_c\sin\psi + z \end{cases} \\ \sin\psi z' - \left(\cos\psi\sin\upsilon z' + \cos\upsilon S'_g\right)z'_c \\ -\left((a+S_g)z'_c\sin\upsilon\sin\psi + \cos\psi\left(a + x_c\cos\upsilon + S_g + z_c z'_c\cos\upsilon\right)\right) = 0 \end{cases} \tag{44}$$

The more detailed expressions of Eq. (44) corresponding to the truncated-cone and spherical surfaces are disregarded so that this paper is not too lengthy.

8 Computer simulation of compensation and its practical manufacturing

The following example is presented to illustrate the result of utilizing the proposed manufacturing model and the system-

atic modeling procedure of grinding the manufacturing model for this special cutter. According to the cutting-edge curve design model and the geometry model of the cross-section profile of the helical flute of the section 2 to 7, each geometrical parameter is substituted by the practical data from Table 1 and Eqs. (1), (8), (10), (17) to find the cutting-edge curve of the four-edge truncated-cone ball-end cutters. From Fig. 6, the helical cutting-edge curve is continuous based on the different revolution faces. From Table 2, the curve of the groove shaped cross-section can be obtained as Fig. 7.

The cross-section curve of the grinding wheel can be obtained from the design parameters of the groove shaped cross-section curve, Eqs. (25) and (29).

The cross-section curve of the grinding wheel is shown in Fig. 8. The computer simulation model of the grinding wheel shows as Fig. 9, which is produced with PRO/E and CAD software.

Finally, the computer practical model file (.PRT) is transferred into CNC as a readable file (.IGS) to finish the prototype of the practical grinding wheel shown as Fig. 10. Based on the combination of the modification of the radial-direction feeding velocity, angular velocity, and axial-direction feeding velocity for grinding wheel and relative movement with the milling cutter, the position and direction of the grinding wheel in the moving coordinate of the milling cutter can be obtained from Eqs. (43) and (44). Residual material between the adjacent flutes and lack of land in part of the flute are shown Fig. 11 and Fig. 12.

In order to finish the residual material and rebuild the land of the cutter, we have developed a compensation technique, which is shown in Fig. 13. The geometric parameters and coordinate system of the grinding wheel, used for compensation are given in Fig. 13. According to the relative positions of points (x, y) on the designed cutting edge and the points (x^*, y^*) on the practical cutting edge, a new grinding wheel with coning angle of $2\alpha_e$ (α_e , relief angle) should be used for the compensation. Keeping the revolving velocity ω and the axial velocity v_z unchanged modifies the radial velocity v_g with the factor of ρ.

$$x(\rho x - x^*) + y(\rho y - y^*) = \sqrt{x^2 + y^2}\sqrt{(\rho x - x^*)^2 + (\rho y - y^*)^2}\sin\alpha_e \quad (45)$$

8.1 The radial velocity v_g is defined by

$$v_g = \rho\frac{d\left(\sqrt{x^2 + y^2}\right)}{dt} \quad (46)$$

After such compensation, the residual material can be diminished. From the above discussions and the simulation results, the manufacturing models for design and NC machining of revolving cutters are more reliable and acceptable.

According to the machining theory derived in this paper, the machining test is conducted by using a modified grinding wheel path on a WALTER CNC grinding machine. Figure 14 shows the original model of the toroid-cone shaped cutters of test. Test result shows the accuracy and reliability of the theory model in this paper.

9 Conclusion

From the previous models, simulated results, modifications, post-process and realization of the grinding wheel section, it is obvious that the detailed models of truncated-cone ball-end cutter are provided. The major contributions of this work include:

1. To present a systematic method for design and manufacturing of the truncated-cone ball-end cutter.
2. To present the geometry and manufacturing models for helical cutting-edge curve.
3. To obtain the geometry and manufacturing models for a helical flute and grinding wheel by solving the inverse envelope problem of given flute profile.
4. To present the equations of axial, rotary, and modified radial feeding velocity for workpiece and grinding wheel.
5. To present the technique for compensation to finish the residual material and rebuild land of cutter.
6. The machining of this kind of cutter is finished by a 2-axis NC machine so that the manufacturing cost can be reduced effectively.

The results of numerical experiments indicate that the proposed modeling method is feasible and reliable.

References

1. Batlle JA, Cardona SC, Sanz VN (1985) On the Design of Milling Cutters or Grinding Wheels for Twist Drill Manufacture A CAD Approach. Proc Of the 25th Int MTDR Conf 25:315–320
2. Bedi S, Gravelle S, Chen YH (1997) Principal Curvature Alignment Technique for Machining Complex Surfaces. J Manuf Sci Eng Trans ASME 119:756–765
3. Choi BK, Jun CS (1989) Ball-End Cutter Interference Avoidance in NC Machining of Sculptured Surfaces. Comput-Aided Des 21 (6):371–378
4. Ehmann KF (1990) Grinding Wheel Profile Definition for The Manufacture of Drill Flutes. Ann CIRP 39(1):153–156
5. Elber G (1995) Freeform Surface Region Optimization for 3-Axis and 5-Axis Milling. Comput-Aided Des 27(6):465–470
6. Kang SK, Ehmann KF, Lin C (1996) A CAD Approach to Helical Flute Machining-I. Mathematical Model and Model Solution Int J Mach Tools Manuf 36(1):141–153

7. Li LF (1995) Calculating the Normal Section of Helical Flute of the Cutter by Computer. Tool Eng 9:15–19
8. Liu JY, Liu HM (1997) The Mathematical Model of Helical Flute of Cone-type Ball-end Cutter. Tool Eng 4:3–6
9. Sheth DS, Malkin S (1990) CAD/CAM for Geometry and Process Analysis of Helical Flute Machining. Ann CIRP 39 (1):129–132
10. Tang YY, Cheng CK et al (1996) Geometry Model and 2-axis NC Machining of Milling Cutters with Constant Helical Angle. J Harb Instit Technol 28(5):5–7
11. Zhang H, Yao NX et al (1997) The General Algorithm of Cutting Edge of Revolving Cutter with Constant Helical Angle. J Dal Instit Technol 37(1):63–67
12. Tsai YC, Hsieh JM (2001) A Study of A Design and NC Manufacturing Model of Ball-End Cutters. J Mater Process Technol 177:183–192
13. Chen W-F, Lai H-Y, Chen C-K (2002) Design and NC Machining of Concave-Arc Ball-end Milling Cutters. Adv Manuf Technol 20 (3):169–179
14. Chen W-F, Lai H-Y, Chen C-K (2001) A Precision Tool Model for Concave Cone-End Milling Cutters. Adv Manuf Technol 18 (8):567–578
15. Chen W-F, Lai H-Y, Chen C-K (2002) A Comprehensive Engineering Model for the Design, Manufacture and Assembly of Helical Carpenter Shapers. Proc Inst Mech Eng, B J Eng Manuf 216(11):1493–1504
16. Chen W-F, Lai H-Y, Chen C-K (2003) Quality Assurance for Concave-Arc Ball-End Milling Cutters. Proc Inst Mech Eng, B J Eng Manuf 217(2):181–191
17. Tsai YC, Hsieh JM (2005) An analysis of cutting-edge curves and machining performance in the Inconel 718 machining process. Int J Adv Manuf Technol 25:248–261